Journal of Machine Engineering, 2026, Vol. 26
ISSN 1895-7595 (Print) ISSN 2391-8071 (Online)

Received*: 27 March 2026* /Accepted: *11 May 2026* / Published online: *26 May 2026*

mechanical test,
WAAM, DED,
thick-walled components

Abhishek Kumar GUPTA[1,2*], Ali MADEN[3],
Clea PLOUZE[4], Philippe FERAUD[4],
Catherine DA CUNHA[5], Matthieu RAUCH[2],
Helene SAPARDANIS[1]

MECHANICAL ANALYSIS OF THICK-WALLED LOW-CARBON STEEL STRUCTURES PRODUCED BY WIRE ARC ADDITIVE MANUFACTURING WITH ZIG-ZAG TRAJECTORIES

This study investigates the mechanical properties of multilayer thick WAAM components using a zigzag deposition strategy. Four different low carbon steel (ER70S-6) walls with two deposition angles and two turning radii were evaluated. The comprehensive design of experiment focuses on microstructural analysis and mechanical properties, including hardness, tensile strength, and Charpy V-Notch (CVN). Non-destructive Testing (NDT), including ultrasound and radiography, was also performed to assess the integrity of the wall. The fracture surfaces from CVN and tensile test samples were examined with Scanning Electron Microscope. The results reveal a negligible anisotropy of global mechanical properties and a limited influence of deposition angle and turning radius. Overall, CVN results have shown ductile failure with a few brittle outliers. These results suggest that the selected deposition strategy does not have a significant effect on global mechanical properties, which showed an isotropic behaviour. Nevertheless, the CVN outliers underline the critical role of local microstructural heterogeneities in fracture toughness. These findings contribute to the characterisation of the WAAM process for thick parts.

1. INTRODUCTION

Additive manufacturing (AM) is a novel manufacturing technique that enables the creation of complex and customised 3D objects by depositing material layer by layer. Although its first applications mostly consisted of decorative objects and nonfunctional prototypes, AM and especially Metal AM have become a real alternative to conventional manufacturing processes thanks to the significant advancements in recent years [1]. Offering

[1] SNCF, DTIPG, France
[2]Nantes Université, École Centrale Nantes, CNRS, GeM, UMR 6183, F-44000 Nantes, France
[3] Ingenierie du Materiel – , SNCF Voyageurs, France
[4] Ingenierie du Materiel – Agence d'Essai Ferroviaire (AEF), SNCF Voyageurs, France
[5] Nantes University, École Centrale Nantes, CNRS, LS2N, UMR 6004, F-44000 Nantes, France
[*] E-mail: abhishek-kumar.gupta@ec-nantes.fr
https://doi.org/10.36897/jme/221668

design freedom, customisation, time and material efficiency, AM has expanded its applications across various industries. According to EN ISO/ASTM 52900 [2], Directed Energy Deposition (DED) is one of the seven categories of AM encompassing processes in which concentrated thermal energy is used to melt and deposit material. Among DED processes, Wire Arc Additive Manufacturing (WAAM) emerges as one of the most promising, which needs less maintenance and build cost compared to laser-based technology. WAAM also offers higher deposition rates (5-10 kg/h) compared to other technologies [3]. The process is based on arc welding, with an electric arc as a heat source and welding wire as feedstock [3]. It has different variants like plasma arc (PAW), gas tungsten arc (GTAW) and Gas Metal Arc (GMAW), the last being the most widely used [1].

WAAM has witnessed an increasing interest from researchers and industry in the last decade, as it enables Maintenance, Repair, and Overhaul (MRO) production of complex parts with less material compared to conventional manufacturing processes like forging and, casting [4–7].

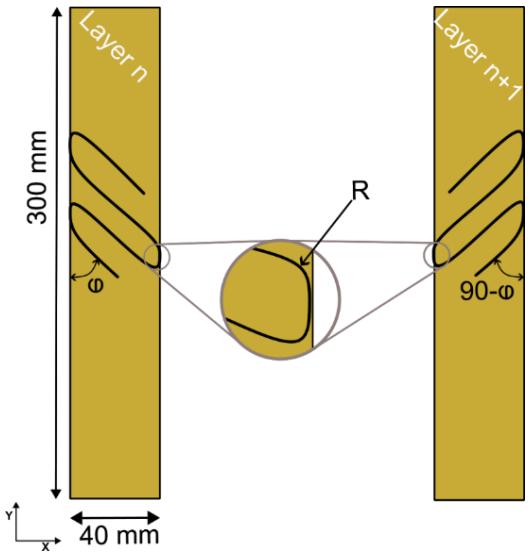

Fig. 1. Schematic representation of the wire deposition trajectories and layer start points for consecutive layer n, n+1 for $\theta = +/-45^{\circ}\& +60^{\circ}/-30^{\circ}$deg

Despite the advantages, WAAM presents a significant number of challenges to overcome for widespread industrial use of this technology. The mechanical properties of WAAM parts depend on the printing strategy, process parameters and part geometry. These three aspects, which are interdependent, have been widely explored by various studies to evaluate the mechanical performance as well as the dimensional accuracy.

The set of process parameters used has a direct influence on the microstructure of the part, which defines its mechanical behaviour. Researchers have focused on optimising the individual input process parameters like shielding gas flux [8], wire feed speed (WFS), travel speed (TS), interlayer cooling time [3] and, preheat temperature [9], to characterise the mechanical performance [3, 9–12] and the residual stresses induced due to multiple thermal cycles [13].

For a given part, its geometry and dimensions highly limit the number of feasible printing strategies. Therefore, it should be modelled with anticipation with each other. Several printing strategies have been proposed for thin (single bead) and thick (overlapping, spiral, oscillating, etc.) walls.

In the case of thin walls, Huang et al. [14] compared two single bead walls, with a thickness of 3 mm and 8 mm. Compared to the nominal properties of the filler metal, the WAAM process resulted in a decrease of both the yield strength and ultimate strength by about 30% and 20% for 8 mm and 3 mm walls respectively. Le et.al [15] have also investigated the thin walls and concluded that the alternating deposition strategy produces a more regular layer height.

Uyen et al. [16] tested four different infill patterns on a thick (16 mm) mild-steel and found that the spiral trajectory gives the best results with respect to microstructure and tensile strength. Whereas, Iturrioz et al. [17] obtained the best tensile test results with the zigzag strategy on a similar study on Invar36. Moore et al. [10] presented a comprehensive study of stainless-steel and carbon steel. Charpy impact tests were conducted on different printing strategies, and an oscillating pattern resulted in better results.

However, studies on thick walls and their effects on the microstructure, mechanical properties, including Charpy-V impact toughness properties, are less explored [14, 16–21]. Especially, there is a gap in literature concerning thicker (>30 mm) structures with a weaving strategy. Therefore, this paper presents a detailed analysis of the microstructure, including SEM images of the fracture surfaces and the mechanical properties of thick-wall (40 mm) WAAM low-carbon steel (LCS) samples. Here, the zigzag strategy was selected because, as concluded by Ozaner et al. [22], it helps mitigate warping and distortion by balancing heat distribution across layers, thereby reducing deformation. Furthermore, a variation in radii of curvature is introduced to study its effect on surface texture. This analysis is crucial for the design and validation of large-scale components with thick cross sections commonly found in industries like maritime, oil and gas and railway applications [3, 23, 24].

2. EXPERIMENTAL PROCEDURES

An analysis comparing four walls, each produced using a zigzag deposition strategy with two angles (45° and 60°) and two radii of curvature (R) in the turning zones (R = 0.5 mm and R = 1.2 mm) is presented. The schematics of the strategy are shown in Fig 1. All walls are fabricated at the maintenance site of SNCF in Saintes, France, using a COMAU N-220 Robot with 6-axis articulated robot with a 2-axis positioner, CMT welding generator Fronius® TPSi 400 (Fig. 2).

The nominal wall dimensions were 300 mm × 250 mm × 40 mm, with an average layer height of 2.7 mm, deposited on S235JR structural steel plates with dimensions of 400 mm × 250 mm × 25 mm. The LCS wire used in the experiments is Castolin 45202 G3Si (EN ISO 14341-A: G42 4M21 3Si, AWS A5.18: ER70S-6) [25] with 1.2 mm, whose chemical composition and mechanical properties are given in Table 3, as provided by the manufacturer.

The ER70S-6 steel wire is chosen because of its low cost, its good weldability and its widespread use in the welding of LCS alloys in various industries, including rail transportation (rolling stock maintenance). The key process parameters which were held

constant during the experiments are given in Table 1. To ensure optimal welding conditions, the substrate plates were prepared by sandblasting to remove any oxide layers and were cleaned with alcohol to eliminate contaminants. The plates were then clamped to avoid deformation during the welding process. Before deposition, the substrate plates were preheated using a ceramic resistance heating pad to an initial temperature of approximately 140°C to 150° C.

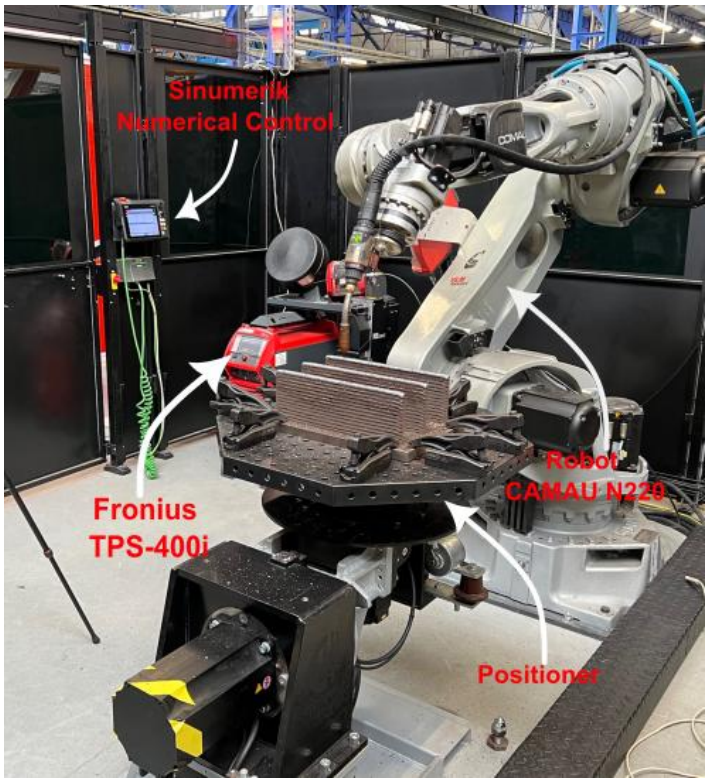

Fig. 2. WAAM experimental setup

Fig. 3. Wall after printing–W60R05

Table 1. Welding parameters used in the study

Parameter	Value
Welding mode	CMT- Gap bridging
Wire feed speed (WFS)	6.5 m/min
Current (A)	223
Voltage (V)	14.3
Travel speed (TS)	1000 mm/min
Contact tip to workpiece distance (CTWD)	13 mm
Shielding gas	M21ArC18 - 14 L/min
Interlayer temperature	185°C
Preheat temperature	140°C–150°C

Table 2. Wall angle and radius parameters

Wall	Θ (deg)	R (mm)
W45R05	45°	0.5
W60R05	60°	0.5
W45R12	45°	1.2
W60R12	60°	1.2

Table 3. Wire material composition – ER70S

M	C	Mn	Al	Si	S	P	Cu	Mo	Ni	B	Ti	Ti+Zr	N	V	Cr
%	0.08	1.49	0.003	0.88	0.016	0.012	0.01	0.01	0.02	0.0004	0.002	0.012	0.004	0.003	0.01

Four walls with different configurations were fabricated as presented in Table 2. W60R05 is shown in Fig. 3. The robot followed a zigzag trajectory with a rotation of 90° of the weaving angle between each layer. Moreover, the start and end points of each layer were alternated between the four corners of the wall to avoid the build-up of geometric irregularities and to provide a more homogeneous heat distribution. The welding torch was kept perpendicular to the substrate, maintaining an average contact tip-to-work distance (CTWD) of 13 mm with an average layer height of 2.7 mm. The heat input was 0.15 kJ/mm, which is calculated using Eq (1), where Q is the heat input, ε is the thermal efficiency of the welding process (taken as 0.8 for MIG/MAG welding), V is the arc voltage (Volts), I is the arc current (A), and S is the Travel speed (mm/min).

$$Q = \varepsilon V \left(\frac{I}{S}\right) \tag{1}$$

Following the deposition, all walls received a stress-relieving heat treatment before NDT and sample preparation. First, the surface texture of the walls was captured by a 3D scanner GOM ATOS Q and compared, as presented in Fig. 5. The analysis included NDT and mechanical testing.

In the case of NDT, Ultrasonic Testing (UT) was used to evaluate the interface between the substrate and the wall, to detect the lack of fusion and insufficient weld penetration by using M2M Gekko machine at Agence d'Essai Ferroviaire (AEF), Paris, France. The internal defects, such as porosity and inclusions, were analysed by Radiographic testing (RT) over the YZ section of the walls by an external supplier.

To assess the mechanical properties, hardness, tensile, which were performed at AEF. The Charpy impact tests (-40° C) were conducted on samples extracted from the walls by the external supplier. The distribution of different samples on the wall is presented in Fig. 4. The first printed wall (W45R05) (Fig. 4.a) contains 33 cylindrical tensile specimens, 21 V-notch Charpy specimens, and 2 macro hardness specimens. The three other walls each have 13 cylindrical tensile specimens, 12 V-notch Charpy specimens, and 1 macro hardness specimen.

Due to the observed homogeneity and isotropy of the results of W45R05, the number of samples to be extracted from W60R05, W45R12 and W60R12 was reduced to simplify the analysis.

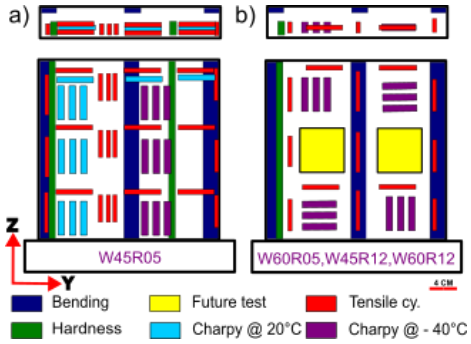

Fig. 4. Schematics of Sample Extraction Planning for W45R05 (b)W60R05, W45R12 and W60R12

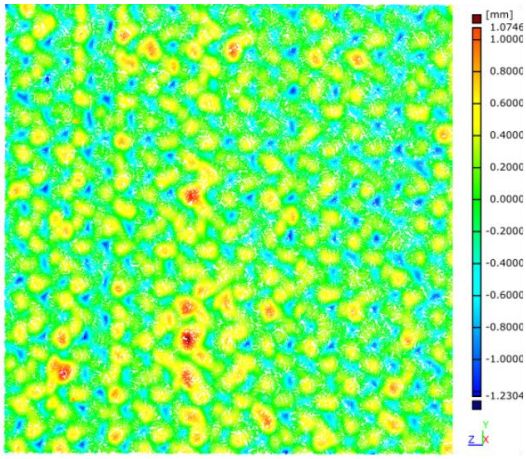

Fig. 5. Wall Texture scanned by 3D scanner W45R12

3. RESULTS

In this section, the results of the above-described experiments are presented and compared for each wall.

3.1 SURFACE TEXTURE

Fig. 5 shows a patch of scan data from the mid-zone of W60R12. Overall, all four walls exhibit a similar level of surface waviness without significant variations between strategies.

3.2. NDT

3.2.1. ULTRASONIC TESTING (C-SCAN)

A multi-element ultrasonic C-scan inspection was performed to evaluate the integrity of the substrate–wall interface. A minimum recordable indication diameter of 3 mm was adopted, based on calibration with reference blocks. The probe was positioned on the bottom surface of the substrate to acquire (Fig. 6) the C-scan maps shown in Fig. 7. No significant indications were detected in any of the walls by ultrasonic testing.

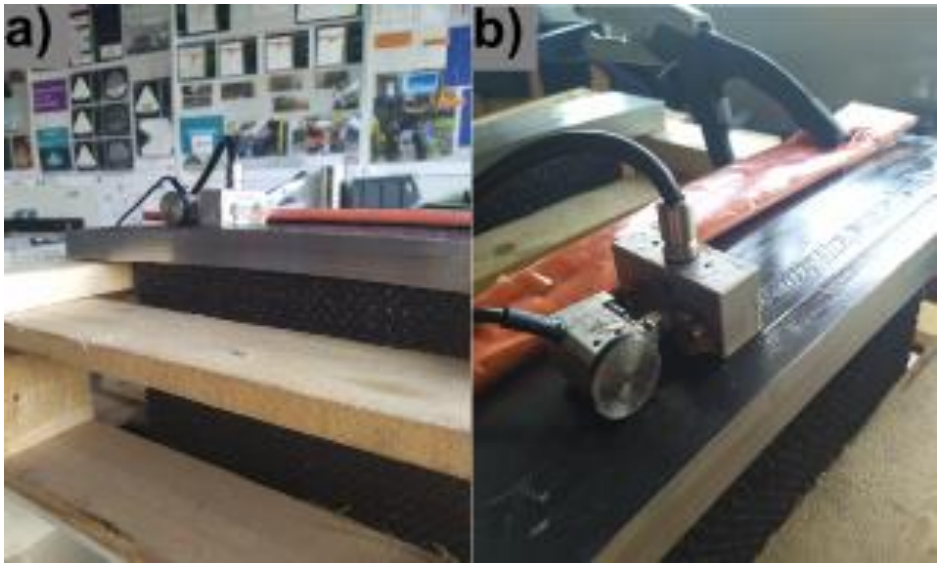

Fig. 6. Ultrasound Test procedure a) Side view b) Top view

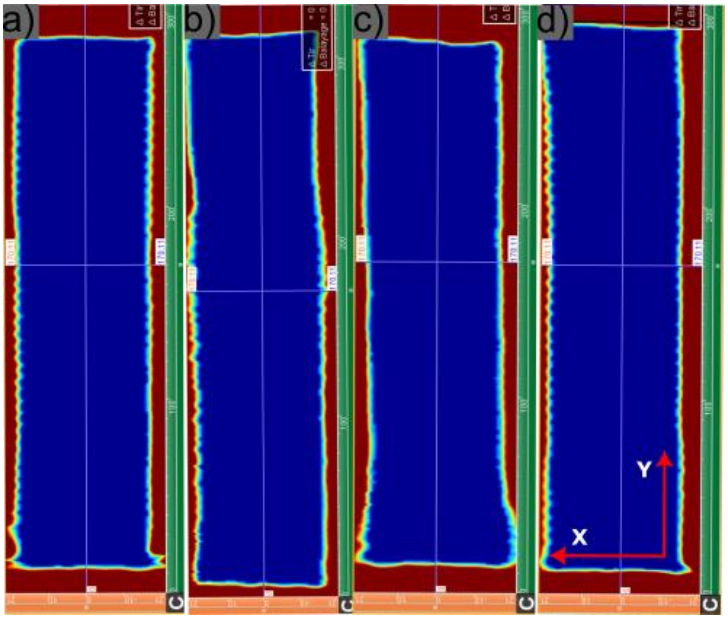

Fig. 7. C-Scan result of for wall a) W45R05 B) W60R05 C) W45R12 D)W60R12

3.2.2. RADIOGRAPHIC TESTING

Radiographic tests were conducted according to the NF EN ISO 17636-1 [26]. The minimum detectable defect size was 0.6 mm. In W45R05 and W60R05, no defects were detected. In W45R12 and W60R12, a spherical porosity of 1.5 mm was detected in the mid-height zone. The defect is assumed to be caused by a process interruption or gas flow variation during the manufacturing process.

3.3. HARDNESS TEST

Vickers (HV10) hardness tests were conducted according to NF EN ISO 6507-1 [27]. The test specimen was divided into 6 zones along the build direction (z-axis). In each zone, multiple measurements were taken both along vertical (z-axis) and horizontal (x-axis) directions for all walls. Fig 8 shows these points of measurement for W45R05 at mid-height.

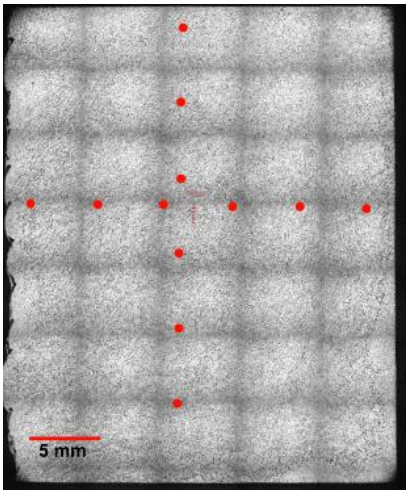

Fig 8. Hardness measured points for W45R05

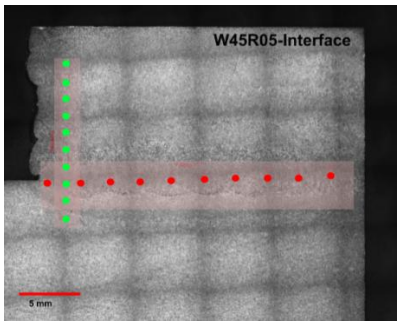

Fig 9. Hardness points at the interface for the w45r05

For W45R05 and W60R05, the maximum hardness values were found near the interface or in the first few layers of deposition. In contrast, the hardness measurements for W45R12

and W60R12 are quite homogeneous along the height. Average hardness values of all walls are also presented in Fig. 11, where error bars represent ±2 standard errors, corresponding to 95 percent confidence interval. For the W45R05, the hardness was also measured at the interface, as presented in Fig 9, the measured values for vertical and horizontal profiles are presented in Fig. 10.

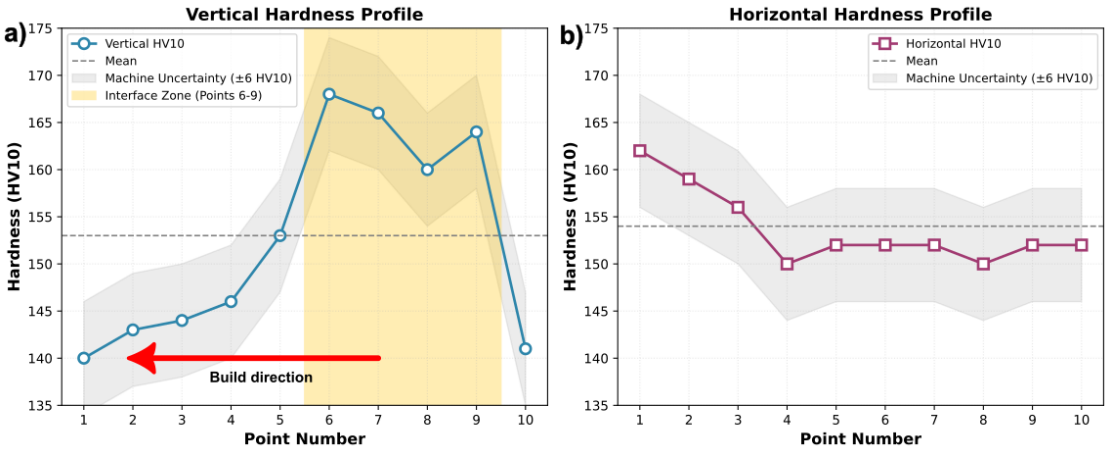

Fig. 10. Hardness values of W45R05 at the interface b/w substrate & first layers: a) Vertical, b) Horizontal

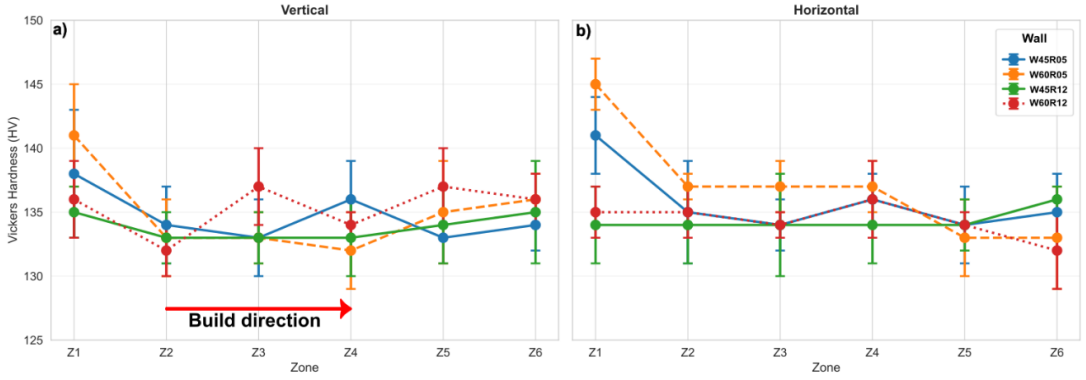

Fig. 11. Average Hardness value comparison for all walls: a) Vertical, b) Horizontal

3.4. TENSILE TEST

The tensile tests were conducted according to NF EN ISO 6892-1 [28] using specimens with a 6 mm diameter and 57 mm gauge length. The tensile strength (MPa), yield strength (MPa) and percentage elongation (A%) were compared for all cases. Overall, the tensile strength (459-471 MPa) and yield strength (305-328 MPa) values were homogeneous and isotropic across all walls and zones, as presented in Fig. 12, Fig. 13 and Fig. 14, where error bars represent ±1 standard deviation. Elongation at fracture was uniform in the Y direction for all parameter sets, but in the Z direction, the wall presented a significant variation in percentage elongation along its height, one of W60R05 is presented in Fig. 15.

SEM analysis of the tensile fracture surfaces confirmed ductile fracture behaviour across all specimens, characterised by the presence of equiaxed dimples presented in Fig. 16. The fracture surfaces exhibited similar morphology regardless of the build parameters used, suggesting that the fundamental fracture mechanism remained consistent despite variations in elongation values between the *Y* and *Z* directions. This dimple pattern is typical of ductile failure in LCS and correlates with the good elongation values obtained during testing. No clear trend in strength or ductility could be directly attributed to the weaving angle or *R*.

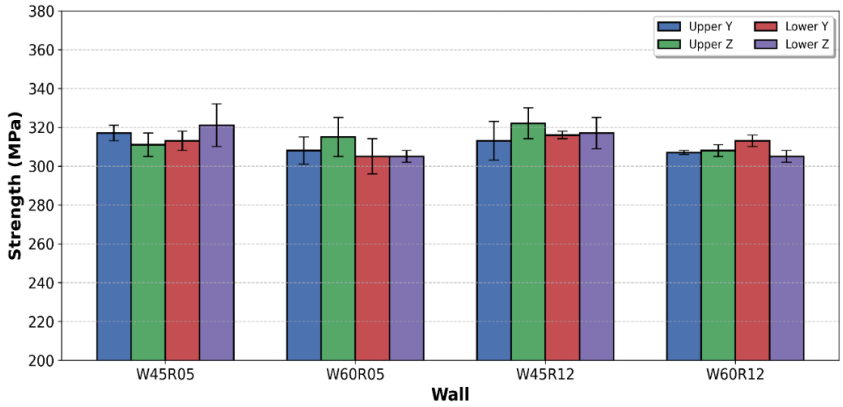

Fig. 12. Yield strength comparison for the upper and lower zones

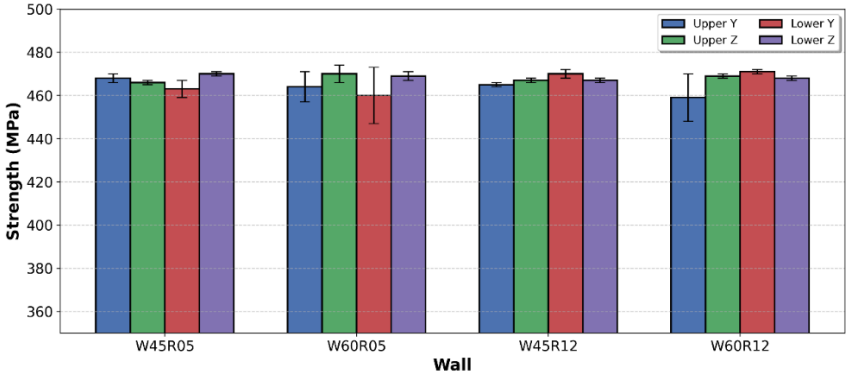

Fig. 13. Ultimate Tensile strength comparison of the upper and lower zones

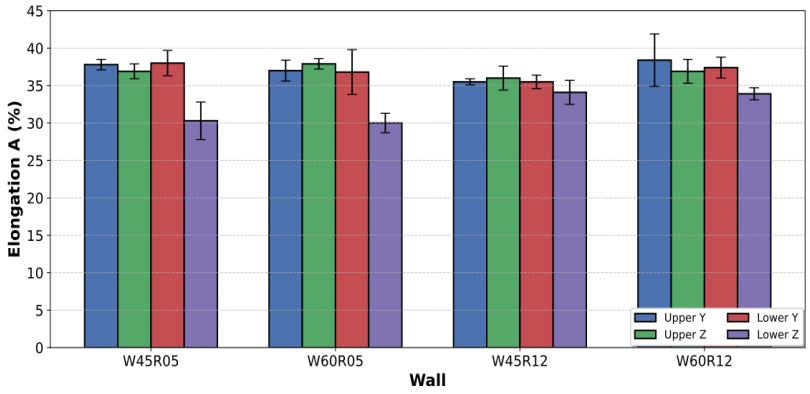

Fig. 14. Elongation deformation comparison of the upper and lower zones

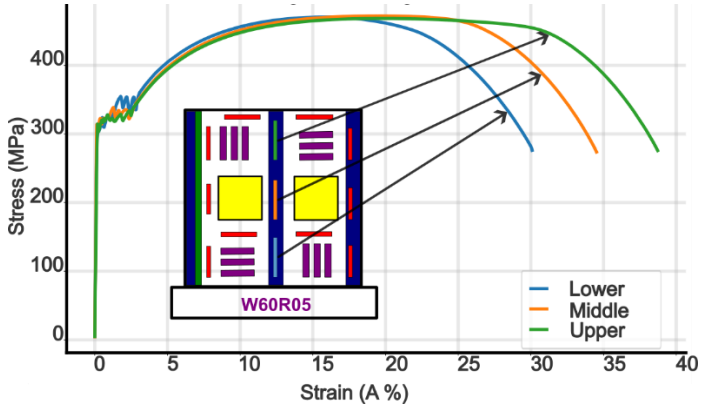

Fig. 15. Tensile Test result along the vertical

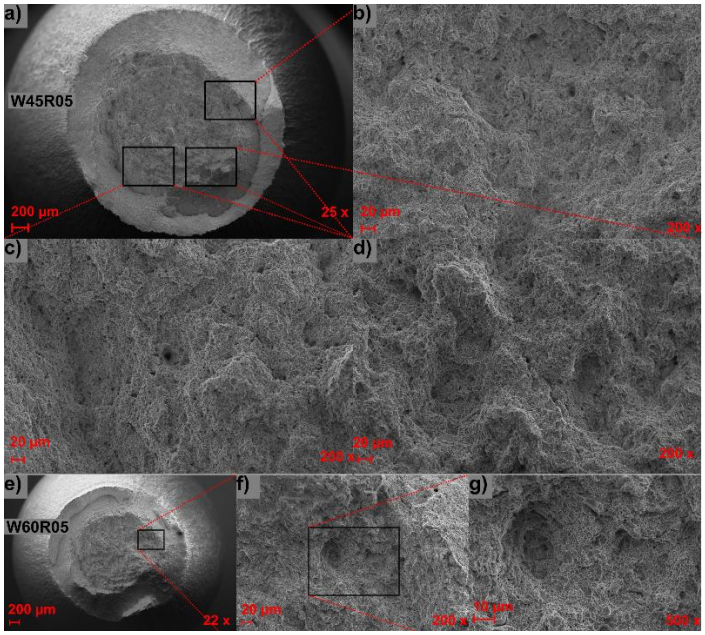

Fig. 16. SEM analysis of the tensile fracture specimen W45R05 and W60R05

3.5. CHARPY V-NOTCH (CVN) TEST

Two impact tests were conducted: one at ambient temperature (~20°C) and another at (-40°C) according to the NF EN ISO 9016 [29] and NF EN ISO 148-1 [30], using V notches with 2 mm depth. The obtained values were compared to the requirements of the EN ISO 14341 [25], which specifies a minimum absorbed energy of 47 J for the filler metal G42 4M21 3Si in the as-welded condition. Specimens from both upper (U) and lower (L) wall zones, in the Y and Z build directions, were compared among all four walls.

The absorbed energy demonstrated appreciable variability across locations, ranging from 134 J to 260 J on average in the Y direction and from 123 J to 303 J on average in the *Z* direction. While most specimens exhibited sufficiently high toughness, certain specimens, particularly U-W45R05 (*Z*) and L-W60R05 (*Y*), showed significantly reduced energy absorption, with values lower than 47 J.

SEM analysis of the fracture surfaces revealed distinctive morphologies corresponding to the fracture toughness values. High energy specimens (240 J) exhibited predominantly ductile fracture features with deep, well-defined dimples, indicating ductile failure (Fig. 18). In contrast, low-energy specimens (<100 J) from positions L-W60R05(Y) showed mixed mode fracture characteristics with significant areas of quasi-cleavage features and shallow, poorly developed dimples, as illustrated in Fig. 19. High standard deviations in several cases are due to the intrinsic dispersion of the Charpy impact test and the presence of brittle outliers (Fig. 17). In general, the upper zone presented higher and more consistent toughness values, while the lower zone was more prone to variation and occasional low-toughness results.

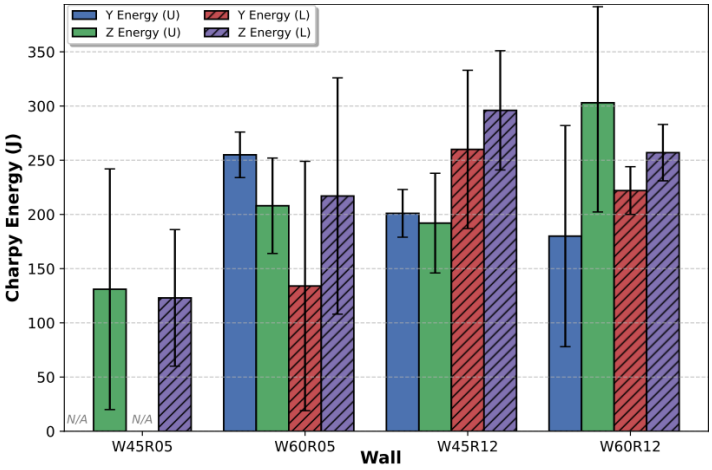

Fig. 17. Charpy Impact energy for all four walls

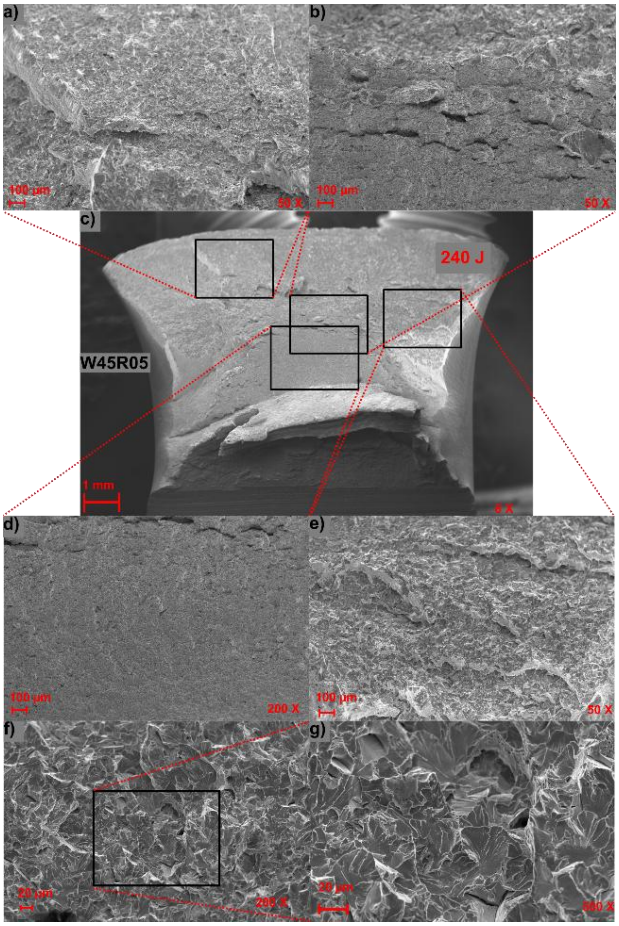

Fig. 18. SEM analysis of Charpy (CVN) specimen for W45R05

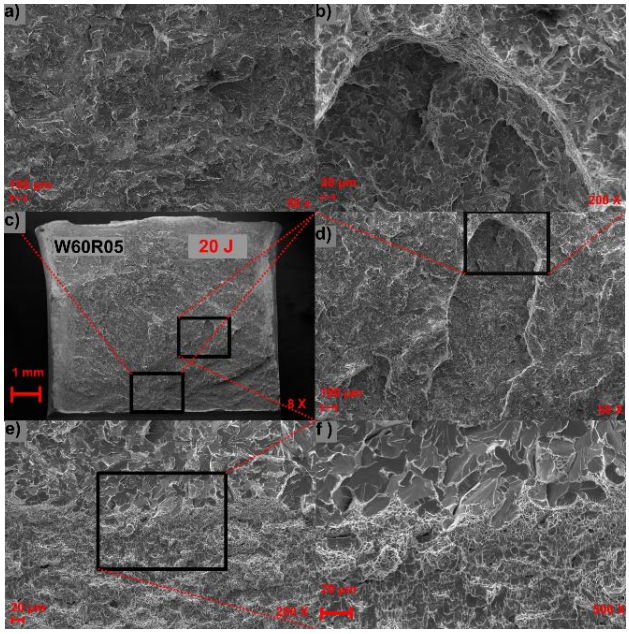

Fig. 19. SEM analysis of Charpy (CVN) specimen for W60R05

3.6. MICROSTRUCTURE

Microstructural examinations were conducted on all four WAAM walls to investigate the influence of deposition parameters on grain morphology and phase distribution. Samples were polished and etched with 4% Nital solution to reveal the micro-structural features. Macrostructural analysis, as shown in Fig. 20, revealed distinct bands corresponding to the individual deposition passes.

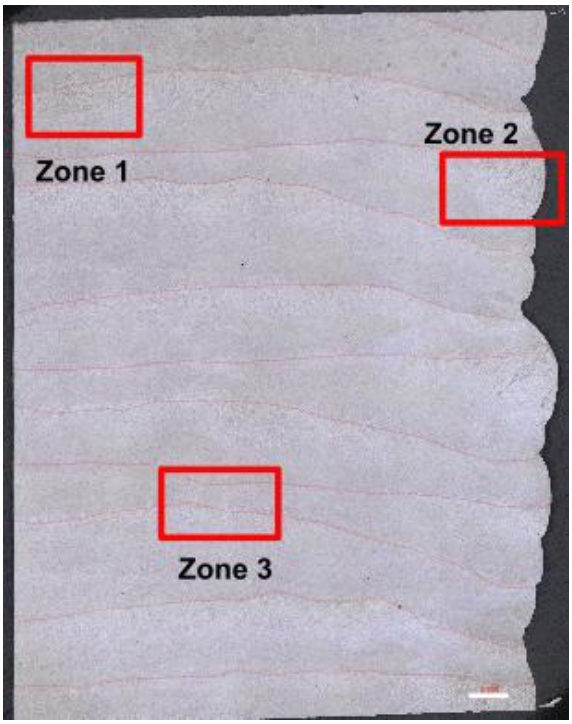

Fig. 20. Macro structure variation over the layer for W60R05 in lower zone

Detailed microstructural examination at higher magnifications (Fig. 21) showed a specific pattern in the variation of grain morphology. Fine equiaxed grains are present at the interface between layers due to the partial remelting of the metal, which is similar to normalising heat treatment. Meanwhile, the middle zones of the layers are not reheated to austenitization temperature (850°C–950°C), and the grains keep their columnar structure inherited from the previous solidification. This changeover of micro-structure along the z-direction is present in all four walls.

The analysis was conducted on 18 microscopic images per wall, 6 lower, 6 middle and 6 upper regions, captured randomly on the samples shown in green in Fig. 4 for all walls. The images were analysed by ImageJ software revealing a maximum porosity ratio smaller than 1% and an average porosity ratio less than 0.5% for all walls. Different weaving angles did not have any significant effect on the porosity ratio.

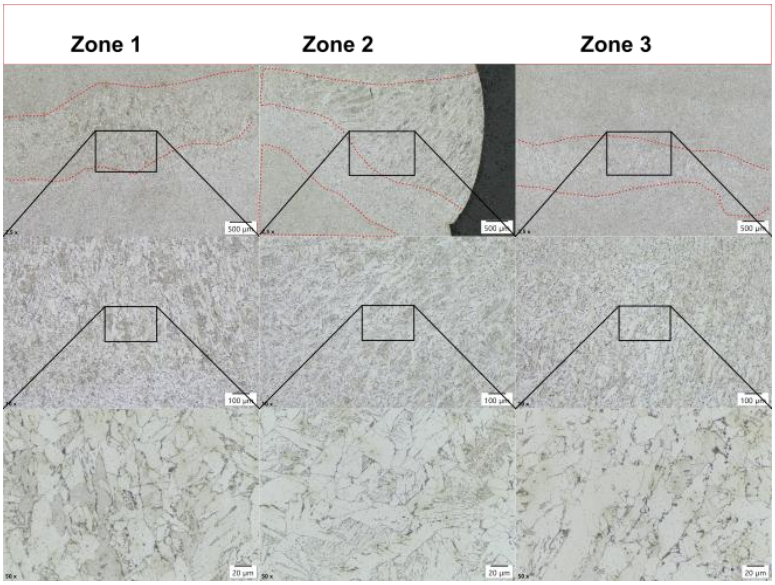

Fig. 21. Microstructure variation over different zones

3.7. POROSITY ANALYSIS

The analysis was conducted on 18 microscopic images per wall, 6 lower, 6 middle and 6 upper regions, captured randomly on the samples shown in green in Fig. 4 for all walls. The images were analysed by ImageJ software revealing a maximum porosity ratio smaller than 1% and an average porosity ratio less than 0.5% for all walls. Different weaving angles did not have any significant effect on the porosity ratio.

These results demonstrate the capacity of WAAM to produce dense parts with minimum porosity. The spatial distribution of porosity ratio varied among the walls, with W60R05 in Fig. 22 showing a concentration of pores primarily in the mid-height region, while the other walls exhibited more uniform distribution throughout the structure.

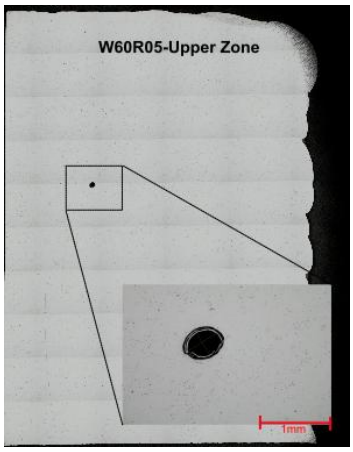

Fig. 22. Porosity in wall W60R05 in upper zone

4. DISCUSSION

The above-mentioned results revealed significant insights into the mechanical properties and microstructure of thick steel walls produced by WAAM process using different strategies. Overall, all four walls gave similar results in terms of mechanical properties and microstructure, indicating a negligible effect of theta and R on the results. Ultrasound and radiographic testing have shown that the walls are free from major internal defects such as cracks and lack of fusion.

Despite the heat sink effect of the substrate during the first layer, ultrasound testing has not revealed any lack of fusion defects at the substrate-WAAM interface. Preheating the substrate has been demonstrated as the most effective method to mitigate defects in LCS WAAM builds [24]. X-ray images have only shown two isolated spherical porosities of 1.5 mm, and all four walls have a <1% average porosity ratio. It is believed that local variations of protection gas flow and residues of contaminants on the filler metal and on the substrate are most likely to be the main sources of porosity. From a mechanical perspective, hardness distribution is homogeneous throughout the height of all walls, with values slightly greater near the substrate, aligning with the findings of previous research [19, 31]. Moreover, no significant difference has been observed in hardness among different walls with respect to the weaving angle. However, the current study revealed lower hardness values compared to bibliography [15, 32, 33].

Tensile test results show that yield and ultimate strengths ($R_{p0.2}$, R_m) are significantly lower than standard properties (R_e>420 MPa & R_m>500 MPa) of the filler metal used, while elongation at fracture frequently exceeds the standard value (20%), a result directly linked to the inherent thermal cycles. Successive reheating of the previously deposited weld metal has an “annealing” effect on the microstructure, which results in reduced hardness and tensile strength and increased ductility. These microstructural modifications directly correlate with the mechanical behaviour observed and agree with the findings of for WAAM-processed steels [19, 31].

Even though the yield and tensile strength showed an isotropic and homogenous distribution with respect to the specimen direction and position, elongation at fracture has an anisotropic behaviour in the lower part of the walls, resulting in lower values of percent elongation in the vertical direction (*Z*) than in the longitudinal direction (*Y*) (Fig. 12, Fig. 13 and Fig. 14). Moreover, an increase of percent elongation has been observed in build direction for specimens extracted in vertical direction (*Z*). This can be attributed to the steep thermal gradients on the wall’s lower part during the early stage of the printing, which can result in anisotropic behaviour. As the wall gets higher, the heat sink effect of the substrate becomes negligible, the temperature distribution along the height of the wall becomes more uniform and the cooling rate decreases.

CVN impact tests at -40°C show that most of the specimens met or exceeded the filler metal standard (>47 J) with few exceptions from W45R05 and W60R05, in accordance with the range found in recent WAAM literature [19, 31]. Fractography and Charpy failure modes indicate mostly ductile fracture with the presence of dimple and only some brittle zones,

confirming the overall toughness and robustness of the manufactured walls under the conditions tested.

Although most samples have shown a clear ductile failure with high fracture toughness values, a few brittle outliers have been observed (Fig. 17). The presence of these outliers can be attributed to the local heterogeneity caused by the alternating equiaxial-columnar grain microstructure. On one hand, long columnar grain boundaries can be preferential sites for intergranular fracture depending on the loading direction [34]. On the other hand, equiaxed-columnar interface can force the cracks to change orientation resulting in increased crack tortuosity and energy dissipation, thus higher toughness values [35,36]. The high standard deviation of the results is due to the intrinsic dispersion of the CVN impact test and to the presence of brittle outliers.

Macroscopic and microscopic examinations demonstrate very low porosity rates (<1%), with most samples showing no notable defects aside from those induced by surface oxidation. These porosity values are well within acceptable industrial limits for WAAM components.

The current study revealed lower hardness, yield and tensile strength values compared to those of the literature on the mechanical properties of LCS WAAM components. Even though the studies have used filler metals of similar properties, the variation in mechanical properties can be attributed to the differences in deposition strategies, process parameters and especially the wall thickness. A decreasing trend of the mechanical strength with increasing thickness, which can be seen in Fig. 23

Further microstructural analysis (grain size and ferrite/pearlite ratio) should be performed to better understand the underlying factors resulted in lower strength values compared to filler wire specification. To complement this study, future work should focus on the fatigue performance of WAAM parts, which is crucial for the validation of the process by demanding industrial applications.

Overall, the combination of microstructural observations, mechanical property results, and NDT indicates that WAAM is a reliable and repetitive method for producing thick steel structures suitable for demanding applications, including those in railways, maritime, and oil & gas sectors.

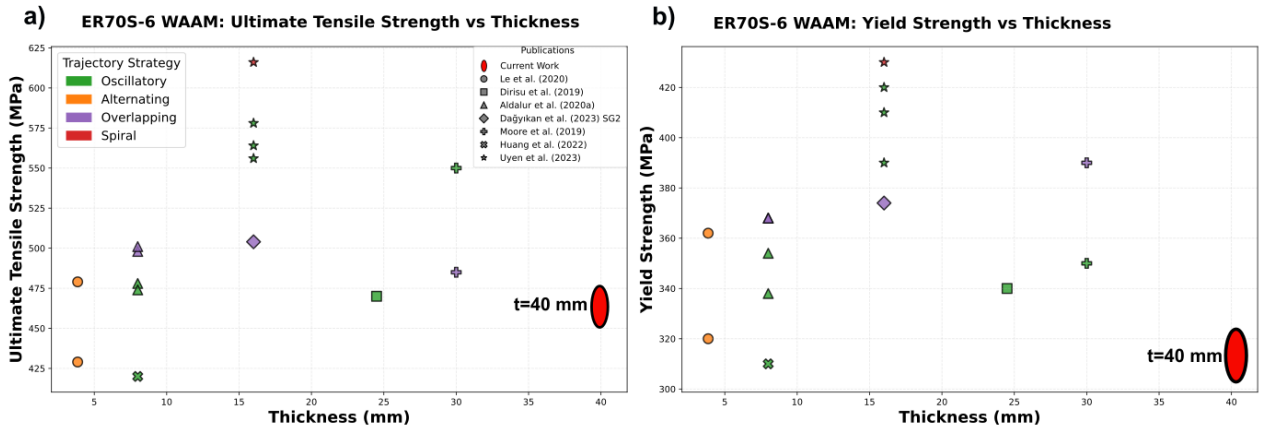

Fig. 23. UTS and Yield strength value comparison for ER70S [10, 14–16, 19, 32, 36]

5. CONCLUSION

This study analysed the microstructure and mechanical properties of four WAAM walls using ER70S-6 filler metal with a zigzag deposition strategy (45°/60° weaving angles; 0.5/1.2 mm turn radius) for producing LCS thick-walled components.

The following conclusions are drawn:

NDT:

- The fabricated walls exhibit exceptionally low porosity (average porosity ratio < 0.5%).
- No significant defects (cracks, lack of fusion) were observed between the substrate - wall interfaces and in the bulk volume of the walls.

Mechanical Properties:

- While ultimate tensile strengths (459–471 MPa) and yield strengths (~305–328 MPa) are below filler metal requirements, the walls largely exceeded the requirement of elongation at fracture (%) values Charpy tests at -40°C reveal predominantly high toughness (>47 J) with few brittle outliers, linked to local microstructural heterogeneities.
- Upper zones show higher toughness, while lower zones exhibit greater variability, underscoring the need for process optimisation to mitigate local brittleness.
- The mechanical properties across different strategies showed similar and repeatable results. This consistency offers more flexibility in trajectory planning as different weaving angles give the same outcome.

Microstructural Analysis:

- The microscopic analysis shows ferrito-pearlitic microstructure of banded regions from successive passes, with equiaxed grains at layer interfaces and columnar grains in mid-layer zones.

Future work should prioritise comprehensive evaluation of fatigue performance. This will enable a deeper understanding of the process and support industries in producing highly functional parts with improved reliability.

ACKNOWLEDGEMENT

This work was carried out within the framework of the Additive4Rail project, funded by BPIFrance. The authors gratefully acknowledge all project partners for their support and technical feedback.

REFERENCES

[1] RAUCH M., HASCOET J.-Y., QUERARD V., MULTIAXIS A., 2021, *Tool Path Generation Approach for Thin Wall Structures Made with WAAM*, Journal of Manufacturing and Materials Processing, 5, 128, https://doi.org/10.3390/jmmp5040128.

[2] *Additive Manufacturing – General Principles – Fundamentals and Vocabulary*, 2025, British Standard is the UK implementation of EN ISO/ASTM 52900:2021, https://doi.org/10.3403/30448424.

[3] QUEGUINEUR A., RÜCKERT G., CORTIAL F., HASCOËT J.Y., 2018, *Evaluation of Wire Arc Additive Manufacturing for Large-Sized Components in Naval Applications*, Weld World, 62, 259–266, https://doi.org/10.1007/s40194-017-0536-8.

[4] WANG L., XUE J., WANG Q., 2019, *Correlation Between Arc Mode, Microstructure, and Mechanical Properties During Wire Arc Additive Manufacturing of 316L Stainless Steel*, Materials Science and Engineering: A751, 183–190, https://doi.org/10.1016/j.msea.2019.02.078.

[5] WILLIAMS S.W., MARTINA F., ADDISON A.C., DING J., PARDAL G., COLEGROVE P., 2016, *Wire + Arc Additive Manufacturing*, Materials Science and Technology, 32, 641–647, https://doi.org/10.1179/1743284715Y.0000000073.

[6] KOKARE S., SHEN J., FONSECA P.P., LOPES J.G., MACHADO C.M., SANTOS T.G., OLIVEIRA J.P., GODINA R., 2024, *Wire Arc Additive Manufacturing of a High-Strength Low-Alloy Steel Part: Environmental Impacts, Costs, and Mechanical Properties*, J. Adv. Manuf. Technol., 134, 453–475, https://doi.org/10.1007/s00170-024-14144-z.

[7] BALIDAS A., KERBRAT O., HASCOET J.-Y., 2024, *The Potential of Additive Manufacturing of Metal Components to Reduce Environmental Impacts*, Journal of Machine Engineering, 24/2, 94–104, https://doi.org/10.36897/jme/186988.

[8] SINGLA J., KUMAR N., BANSAL A., 2025, *Manufacturing of Ti6Al4V Alloy Using Argon Chamber Assisted WAAM-CMT to Avoid Oxidation and Analyses of Mechanical and Metallurgical Properties*, Journal of Alloys and Compounds, 1038, 182950, https://doi.org/10.1016/j.jallcom.2025.182950.

[9] LAMBIASE F., YANALA P.B., PAOLETTI A., 2025, *Thermal, Microstructural, and Mechanical Characterization of Early-Stage Deposition in Wire Arc Additive Manufacturing*, Int J. Adv. Manuf. Technol. 138, 953–970, https://doi.org/10.1007/s00170-025-15561-4.

[10] MOORE P., ADDISON A., NOWAK-COVENTRY M., 2019, *Mechanical Properties of Wire Plus Arc Additive Manufactured Steel and Stainless Steel Structures*, Weld World, 63, 1521–1530, https://doi.org/10.1007/s40194-019-00775-4.

[11] RAUCH M., PIEDRA DORADO J., HASCOET J.-Y., RUCKERT G., 2021, *A Novel Method for Additive Manufacturing of Complex Shape Curved Parts by Using Variable Height Layers*, Journal of Machine Engineering, 21/3, 80–91, https://doi.org/10.36897/jme/138820.

[12] NGUYEN V.C., LE V.T., PHAM N.-L., NGUYEN A.-T., 2023, *Multi-Objective Optimization for Weld Track Geometry in Wire-Arc Directed Energy Deposition of ER308L Stainless Steel*, Journal of Machine Engineering, 23/2/ 123–134, https://doi.org/10.36897/jme/166134.

[13] LAMBIASE F., YANALA P.B., PACE F., ANDREUCCI E., PAOLETTI A., 2025, *Thermal History and Microstructural Evolution in MIG-Wire Arc Additive Manufacturing of Low Carbon Steel: Influence of Key Process Parameters*, Int. J. Adv. Manuf. Technol., 139, 4125–39, https://doi.org/10.1007/s00170-025-16116-3.

[14] HUANG C., KYVELOU P., ZHANG R., BEN BRITTON T., GARDNER L., 2022, *Mechanical Testing and Microstructural Analysis of Wire Arc Additively Manufactured Steels*, Materials & Design, 216, 110544, https://doi.org/10.1016/j.matdes.2022.110544.

[15] LE V.T., MAI D.S., HOANG Q.H., 2020, *A Study on Wire and Arc Additive Manufacturing of Low-Carbon Steel Components: Process Stability, Microstructural and Mechanical Properties*, J. Braz. Soc. Mech. Sci. Eng., 42, 480, https://doi.org/10.1007/s40430-020-02567-0.

[16] UYEN T.M.T., MINH P.S., NGUYEN V.-T., DO T.T., NGUYEN V.T., LE M.-T., NGUYEN V.T.T., 2023, *Trajectory Strategy Effects on the Material Characteristics in the WAAM Technique*, Micromachines, 14, 827, https://doi.org/10.3390/mi14040827.

[17] ITURRIOZ A., UKAR E., PEREIRA J.C., 2025, *Influence of the Manufacturing Strategy on the Microstructure and Mechanical Properties of Invar 36 Alloy Parts Manufactured by CMT-WAAM*, Int. J. Adv. Manuf. Technol., 136, 729–744, https://doi.org/10.1007/s00170-024-14853-5.

[18] DOS SANTOS PAES L.E., DIAS J.M.S., ANDRADE J.R., FILHO E.B., FERRARESI H.N., RIBEIRO DA SILVA L.R., XAVIER DE JESUS SILVA C., BORGES V.L., RIFFEL K.C., HERENU S., FRANCIA P., MAGALHAES E.D.S., LAGARES JUNIOR M.L., RIBEIRO DUARTE C.A., VIEIRA DA CUNHA T., SAAD N.D.S., VILARINHO L.O., 2025, *Comprehensive Experimental and Numerical Characterization of Microstructural and Mechanical Anisotropy in Wire Arc Additive Manufactured Carbon Steel*, Journal of Materials Research and Technology, 36, 7244–7260, https://doi.org/10.1016/j.jmrt.2025.04.318.

[19] DAGYIKAN K., GUROL U., KOCAK M., 2023, *Characterization and Fracture Toughness Evaluation of the Thick-Walled Wire Arc Additively Manufactured Low Alloy Steels*, Weld World, 67, 1009–1019, https://doi.org/10.1007/s40194-022-01424-z.

[20] ZHANG W., LEI Y., MENG W., MA Q., YIN X., GUO L., 2021, *Effect of Deposition Sequence on Microstructure and Properties of 316L and Inconel 625 Bimetallic Structure by Wire Arc Additive Manufacturing*, J. of Materi. Eng. and Perform., 30, 8972–8983, https://doi.org/10.1007/s11665-021-06137-w.

[21] HORGAR A., FOSTERVOLL H., NYHUS B., REN X., ERIKSSON M., AKSELSEN O.M., 2018, *Additive Manufacturing Using WAAM with AA5183 Wire*, Journal of Materials Processing Technology, 259, 68–74, https://doi.org/10.1016/j.jmatprotec.2018.04.014.
[22] OZANER O.C., TALEMI R., TJAHJOWIDODO T., SHARMA A., 2025, *The Influence of the Wire and Arc Additive Manufacturing Parameters on the Surface Irregularities*, Journal of Micromanufacturing, 8, 22–31, https://doi.org/10.1177/25165984241306629.
[23] YA W., HAMILTON K., 2018, *On-Demand Spare Parts for the Marine Industry with Directed Energy Deposition: Propeller Use Case*, M. Meboldt, C. Klahn (Eds.), Industrializing Additive Manufacturing – Proceedings of Additive Manufacturing in Products and Applications – AMPA2017, Springer International Publishing, Cham, 70–81, https://doi.org/10.1007/978-3-319-66866-6_7.
[24] QUEGUINEUR A., ASADI R., OSTOLAZA M., VALENTE E.H., NADIMPALLI V.K., MOHANTY G., HASCOET J.-Y., ITUARTE I.F., 2023, *Wire Arc Additive Manufacturing of Thin and Thick Walls Made of Duplex Stainless Steel*, Int. J Adv. Manuf. Techn., 127, 381–400, https://doi.org/10.1007/s00170-023-11560-5.
[25] NF EN ISO 14341, 2025, Afnor EDITIONS, https://www.boutique.afnor.org/fr-fr/norme/nf-en-iso-14341/produits-consommables-pour-le-soudage-filselectrodes-et-depots-pour-le-soud/fa128781/31693 (accessed September 22, 2025).
[26] ISO 17636-1:2022, ISO, 2025, https://www.iso.org/fr/standard/78319.html (accessed September 19, 2025).
[27] NF EN ISO 6507-1, 2025, Afnor EDITIONS, https://www.boutique.afnor.org/fr-fr/norme/nf-en-iso-65071/materiaux-metalliques-essai-de-durete-vickers-partie-1-methode-dessai/fa182990/80812 (accessed September 19, 2025).
[28] NF EN ISO 6892-1, 2025, Afnor EDITIONS, https://www.boutique.afnor.org/fr-fr/norme/nf-en-iso-68921/materiaux-metalliques-essai-de-traction-partie-1-methode-dessai-a-temperatu/fa197531/84689 (accessed September 19, 2025).
[29] NF EN ISO 9016, 2025, Afnor EDITIONS, https://www.boutique.afnor.org/fr-fr/norme/nf-en-iso-9016/essais-destructifs-des-soudures-sur-materiaux-metalliques-essai-de-flexion-/fa179303/40452 (accessed September 19, 2025).
[30] NF EN ISO 148-1, 2025, Afnor EDITIONS, https://www.boutique.afnor.org/fr-fr/norme/nf-en-iso-1481/materiaux-metalliques-essai-de-flexion-par-choc-sur-eprouvette-charpy-parti/fa182456/58779 (accessed September 19, 2025).
[31] COLEGROVE P.A., COULES H.E., FAIRMAN J., MARTINA F., KASHOOB T., MAMASH H., COZZOLINO L.D., 2013, *Microstructure and Residual Stress Improvement in Wire and Arc Additively Manufactured Parts Through High-Pressure Rolling*, Journal of Materials Processing Technology, 213, 1782–1791, https://doi.org/10.1016/j.jmatprotec.2013.04.012.
[32] ALDALUR E., VEIGA F., SUAREZ A., BILBAO J., LAMIKIZ A., 2020, *Analysis of the Wall Geometry with Different Strategies for High Deposition Wire Arc Additive Manufacturing of Mild Steel*, Metals, 10, https://doi.org/10.3390/met10070892.
[33] ALDALUR E., VEIGA F., SUAREZ A., BILBAO J., LAMIKIZ A., 2020, *High Deposition Wire Arc Additive Manufacturing of Mild Steel: Strategies and Heat Input Effect on Microstructure and Mechanical Properties*, Journal of Manufacturing Processes, 58, 615–626, https://doi.org/10.1016/j.jmapro.2020.08.060.
[34] ZHANG J., FAN J., YANG D., PENG Y., WANG K., 2024, *The Fracture Toughness and Fatigue Crack Growth Properties of 18Ni 300 Maraging Steel Manufactured by Wire + Arc Additive Manufacturing*, Materials Science and Engineering: A, 892, 145993, https://doi.org/10.1016/j.msea.2023.145993.
[35] ZHOU Y., LIN X., JIAN Z., HUANG S., REN Y., WU Y., YANG X., SHAO W., 2023, *Fracture Toughness and Microstructure Damage Behavior of Thin Al–Cu Alloy Fabricated by Wire-Arc Directed Energy Deposition*, Materials Science and Engineering: A, 881, 145420, https://doi.org/10.1016/j.msea.2023.145420.
[36] DIRISU P., GANGULY S., MEHMANPARAST A., MARTINA F., WILLIAMS S., 2019, *Analysis of Fracture Toughness Properties of Wire + Arc Additive Manufactured High Strength Low Alloy Structural Steel Components*, Materials Science and Engineering: A, 765, 138285, https://doi.org/10.1016/j.msea.2019.138285.